




PAPER

[View Article Online](#)
[View Journal](#)

Cite this: DOI: 10.1039/d0dt00733a

Efficient alkane hydroxylation catalysis of nickel(II) complexes with oxazoline donor containing tripodal tetradentate ligands†

Ikumi Terao, Sena Horii, Jun Nakazawa,  Masaya Okamura  and Shiro Hikichi  *

Tris(oxazolynylmethyl)amine TOA^R (where R denotes the substituent groups on the fourth position of the oxazoline rings) complexes of nickel(II) have been synthesized as catalyst precursors for alkane oxidation with *meta*-chloroperoxybenzoic acid (*m*-CPBA). The molecular structures of acetato, nitrato, *meta*-chlorobenzoato and chlorido complexes with TOA^{Me2} have been determined using X-ray crystallography. The bulkiness of the substituent groups R affects the coordination environment of the nickel(II) centers, as has been demonstrated by comparison of the molecular structures of chlorido complexes with TOA^{Me2} and TOA^{tBu}. The nickel(II)-acetato complex with TOA^{Me2} is an efficient catalyst precursor compared with the tris(pyridylmethyl)amine (TPA) analogue. Oxazolynyl donors' strong σ -electron donating ability will enhance the catalytic activity. Catalytic reaction rates and substrate oxidizing position selectivity are controlled by the structural properties of the R of TOA^R. Reaction of the acetato complex with TOA^{Me2} and *m*-CPBA yields the corresponding acylperoxido species, which can be detected using spectroscopy. Kinetic studies of the decay process of the acylperoxido species suggest that the acylperoxido species is a precursor of an active species for alkane oxidation.

Received 27th February 2020,
Accepted 14th April 2020

DOI: 10.1039/d0dt00733a

rsc.li/dalton

Introduction

Oxazoline based compounds have been used as ligands of metal complexes catalyzing various organic transformations including oxidation reactions. For example, the oxazolynyl-phenoxide and oxazolynyl-pyridine ligand complexes of transition metals such as Mn,^{1–3} Fe,⁴ Mo,^{5–7} Pd⁸ and Re⁹ catalyze the oxygenation of alkanes and alkenes with H₂O₂ and *tert*-BuOOH oxidants. Poly(oxazolynyl) ligands have also been employed as the supporting ligands of oxidation catalysts. Enantioselective epoxidation of alkenes with PhIO is catalyzed by a chiral oxazoline ligand complex of iron.¹⁰ Stereoselective allylic oxidation with alkylperoxycarboxylate is mediated by copper complexes supported by chiral oxazoline chelators.^{11–14}

Cobalt(II) complexes with phenyltris(4,4-dimethyloxazolynyl) borate show catalytic alkane oxygenation activity with *meta*-chloroperoxybenzoic acid (*m*-CPBA; HOOC(=O)C₆H₄-*meta*-Cl).^{15,16}

To date, various nickel(II) complexes have been reported as efficient catalysts for alkane hydroxylation with the *m*-CPBA oxidant.^{17–27} The supporting ligands of these nickel complexes comprise nitrogen-donating azoles such as pyridine, imidazole and pyrazole as well as oxygen-donating phenols. As described above, oxazoline derivatives are also expected to be versatile supporting ligands of nickel complexes catalyzing alkane hydroxylation. However, oxazoline based ligands have not been used for nickel complex catalysts activating *m*-CPBA. Notably, 2-oxazolines exhibited π -electron delocalization on the N–C–O segment. An imine nitrogen donor of 2-oxazoline derivatives is expected to be a strong σ -electron donor because of its amido character.²⁸ Therefore, replacement of azoles by oxazolines in nickel-supporting ligands would change the catalytic performance. In this study, we selected tris(2-oxazolynylmethyl)amines, namely TOA^R (where R denotes the substituent groups on the fourth position of the oxazoline rings), as nickel(II) supporting ligands. Electron donation from the ligand would be enhanced by the combination of the tertiary amine nitrogen donor and the oxazolines, which would be favorable for *m*-CPBA activation. TOA^R can be regarded as the analogues of tris(pyridyl-

Department of Material and Life Chemistry, Faculty of Engineering, Kanagawa University, 3-27-1 Rokkakubashi, Kanagawa-ku, Yokohama 221-8686, Japan.

E-mail: hikichi@kanagawa-u.ac.jp; Fax: +81-45-413-9770

† Electronic supplementary information (ESI) available: Data for cyclohexane-*d*₁₂ and toluene oxidation mediated by **1** and **7**, crystallographic data for **1**–**5**, UV-vis spectra of CH₂Cl₂ solutions of **1**–**6**, ESI-MS spectra of MeCN solutions of **1**–**6**, IR spectra of KBr pellets of **1**–**6**, ¹H NMR spectra of **1**, **2**, **4**, **5** and **6**, differential pulse voltammograms of **1** and **7**, time course of total TONs of **1**–**10** in cyclohexane oxidation, and decay of the acylperoxido species in CH₂Cl₂ or CD₂Cl₂ at 25 °C. CCDC 1983778–1983782. For ESI and crystallographic data in CIF or other electronic format see DOI: 10.1039/D0DT00733A

methyl)amine (TPA), in which the pyridine donors are replaced by oxazolines. Notably, the first nickel-based alkane hydroxylation catalyst is the TPA complex reported by Itoh and coworkers.¹⁷

Results and discussion

Synthesis and characterization of Ni(II) complexes with TOA^R ligands

The oxazoline-containing tertiary amines TOA^R have been used as the supporting ligands of metal complex catalysts;^{11,12} however, the molecular structure of the TOA^R complex is reported only for the copper(I) complex with TOA^{Me2}, [Cu^I(TOA^{Me2})₂](BF₄)₂.²⁹ In that dimeric copper(I) complex, TOA^{Me2} bridges two copper centers. The three-coordinated copper(I) center is supported by two of the three oxazolynyl nitrogen donors of one TOA^{Me2} and one oxazoline donor of another TOA^{Me2}; the amine nitrogen of TOA^{Me2} does not coordinate. In this study, therefore, the coordination behavior of TOA^R toward nickel(II) was examined first.

Reacting TOA^{Me2} and NiX₂ in MeOH and adding NaBPh₄ gave the corresponding mononuclear nickel(II) complexes, [Ni^{II}X(TOA^{Me2})](BPh₄), where X = OAc (1), NO₃ (2) and Cl (4) (Scheme 1). These complexes showed paramagnetically shifted ¹H NMR signals attributed to the unpaired electron configuration on the nickel centers (Fig. S4†). X-ray crystallographic analysis revealed their molecular structures. The nickel(II) centers are supported by three oxazolynyl nitrogen donors and the bridgehead amine nitrogen of TOA^{Me2}. In the acetato and nitrate complexes 1 and 2, the anionic ligands are bound to the nickel(II) centers in bidentate mode to give the six-coordinated complexes (Fig. 1(a) and (b), and Table 1). These green-colored complexes showed similar UV-vis spectral patterns involving three weak absorption bands (around 400, 600 and 800 nm; see Fig. S1(a) and (b)†). Conversely, an orange-colored chlorido complex 4 showed absorption bands at 465 nm with medium intensity and at 732 nm with low intensity (Fig. S1(c)†). The observed spectral pattern might be attributed to a distorted five-coordinated nickel(II) center, as evidenced by the crystal structure (Fig. 2(a) and Table 2). The value of a normalized measure of geometry of the five-coordinated center $\tau = 0.59$ indicated that the geometry of the

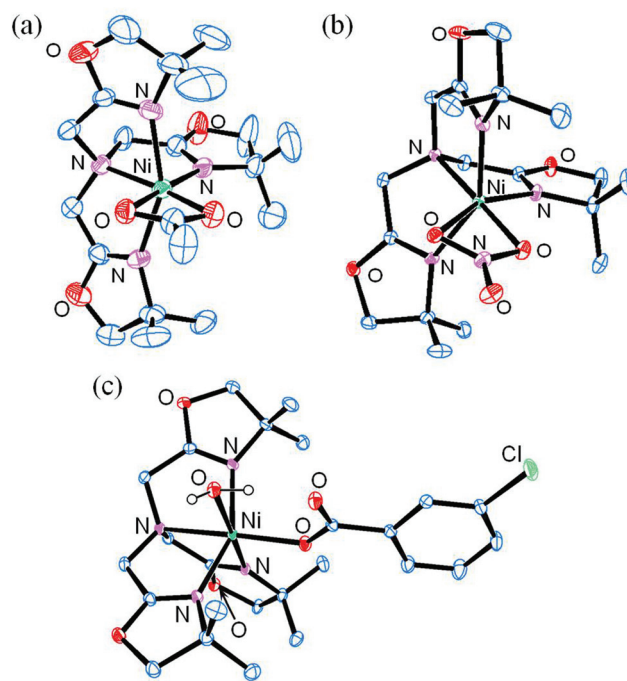
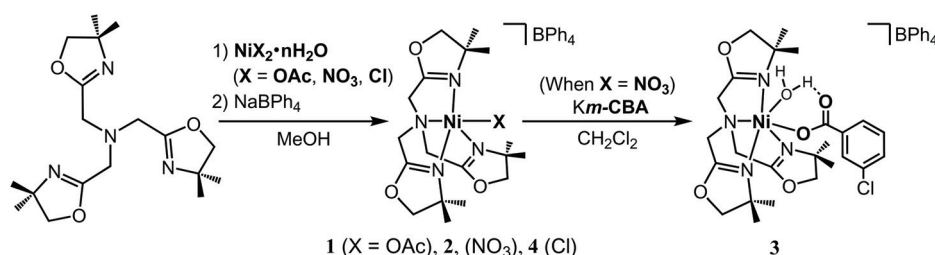


Fig. 1 Crystal structures of the cationic nickel(II)–TOA^{Me2} complex parts of 1 (a), 2 (b) and 3 (c) (30% probability). All hydrogen atoms except the aqua ligand in 3 are omitted.

chloride-bound nickel center was intermediate between a square pyramid ($\tau = 0$) and trigonal bipyramid ($\tau = 1$).

A *meta*-chlorobenzoato (OC(=O)C₆H₄-*meta*-Cl) complex 3 was synthesized by reacting the nitrate complex 2 with the potassium salt of *meta*-chlorobenzoic acid. In complex 3, the nickel(II) center is coordinated by the tetradentate TOA^{Me2}, monodentate carboxylate and H₂O (Fig. 1(c) and Table 1). Intra-molecular hydrogen-bonding interaction between a hydrogen atom of the aqua ligand and an oxygen atom of the carbonyl moiety of *meta*-chlorobenzoate is formed in the crystal structure, as found in the nickel(II)-acetato complex with TPA, [Ni(OAc)(H₂O)(TPA)]⁺ (7).¹⁷

To estimate the structural effects of the substituent groups on the oxazoline rings, TOA^{tBu} and TOA^{Ph} were also employed as the supporting ligands of nickel(II)-chlorido complexes (Scheme 2). The TOA^{tBu} complex 5 was characterized by X-ray crystallography (Fig. 2(b)). The geometry of the five-co-



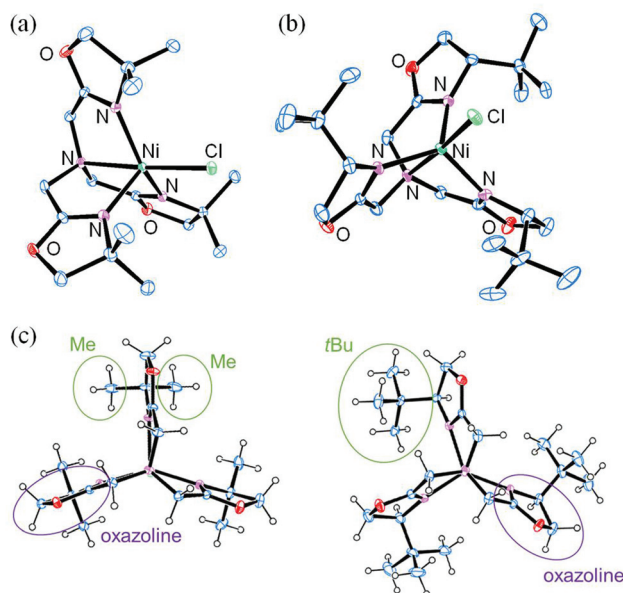
Scheme 1 Synthesis of TOA^{Me2} complexes 1–4.

Table 1 Structural parameters of hexa-coordinated nickel(II) complexes with TOA^{Me2} (1–3)

			3	
Complex	1	2	Molecule 1	Molecule 2
Bond length/Å				
Ni–N1 _{oxazoline}	2.1092(19)	2.061(3)	2.088(2)	2.104(3)
Ni–N2 _{oxazoline}	2.1597(19)	2.071(3)	2.071(3)	2.184(2)
Ni–N3 _{oxazoline}	2.0561(19)	2.033(3)	2.095(2)	2.091(2)
Ni–N4 _{amine}	2.180(2)	2.215(3)	2.200(2)	2.196(2)
Ni–O1	2.0526(19)	2.046(2)	2.019(2)	2.023(2)
Ni–O2	2.1418(17)	2.331(2)	2.171(2) (H ₂ O)	2.132(2) (H ₂ O)
Bond angle/°				
N1–Ni–N2	154.96(8)	147.00(10)	153.19(9)	152.17(10)
N1–Ni–N3	96.49(8)	100.35(11)	96.06(9)	94.72(10)
N1–Ni–N4	80.42(7)	80.48(10)	81.05(9)	80.73(10)
N1–Ni–O1	100.21(8)	101.38(10)	102.30(9)	93.10(9)
N1–Ni–O2	88.75(7)	87.13(9)	87.02(9)	87.91(10)
N2–Ni–N3	93.10(8)	100.56(11)	94.61(9)	96.40(9)
N2–Ni–N4	77.88(8)	77.94(9)	76.57(9)	76.21(9)
N2–Ni–O1	98.41(8)	100.37(9)	102.06(9)	107.74(9)
N2–Ni–O2	85.01(8)	83.29(9)	80.94(9)	79.01(9)
N3–Ni–N4	82.94(7)	80.94(10)	80.46(9)	80.03(9)
N3–Ni–O1	109.01(8)	98.66(9)	90.85(9)	93.10(9)
N3–Ni–O2	171.10(7)	157.32(9)	174.97(9)	174.17(9)
N4–Ni–O1	167.78(7)	178.14(9)	171.01(9)	172.52(9)
N4–Ni–O2	105.10(7)	121.59(8)	96.14(9)	95.29(9)
O1–Ni–O2	62.81(7)	58.73(8)	92.39(9)	91.74(9)

Table 2 Structural parameters of nickel(II)–chloride complexes with TOA^{Me2} (4) and TOA^{tBu} (5)

Complex	4	5
Bond length/Å		
Ni–N1 _{oxazoline}	2.033(3)	2.0553(16)
Ni–N2 _{oxazoline}	2.052(3)	2.0447(17)
Ni–N3 _{oxazoline}	2.020(3)	2.0241(17)
Ni–N4 _{amine}	2.279(3)	2.2218(16)
Ni–Cl	2.3264(12)	2.2517(5)
Bond angle/°		
N1–Ni–N2	140.50(12)	123.61(7)
N1–Ni–N3	103.39(12)	121.11(7)
N1–Ni–N4	80.23(11)	77.96(6)
N1–Ni–Cl	99.07(9)	99.69(5)
N2–Ni–N3	104.96(12)	102.03(7)
N2–Ni–N4	78.28(11)	76.97(6)
N2–Ni–Cl	100.05(9)	102.72(5)
N3–Ni–N4	79.97(12)	78.63(7)
N3–Ni–Cl	104.10(10)	104.58(5)
N4–Ni–Cl	175.91(8)	176.74(5)
τ value	0.59	0.89

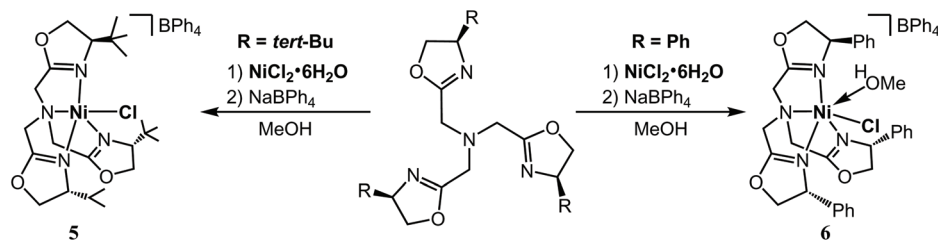
**Fig. 2** Top: crystal structures of the cationic part of the chlorido complexes with TOA^{Me2} 4 (a) and TOA^{tBu} 5 (b) (30% probability). All hydrogen atoms are omitted. Bottom (c): crystal structures of the cationic part of 4 (left) and 5 (right) viewed along the N–Ni axis.

ordinated nickel(II) center is close to trigonal-bipyramid, as indicated by the τ value = 0.89 (Table 2). The view along the Cl–Ni–N axis indicated that the three oxazoline rings linked to nitrogen through methylene spacers appeared in a twisted screw-like arrangement because of the steric repulsion of the *tert*-butyl groups in the pseudo C_{3v} symmetric TOA^{tBu}

(Fig. 2(c)). The solid angle analysis³⁰ of the chlorido complexes revealed the difference in the steric hindrance of TOA^{Me2} and TOA^{tBu}. The equivalent cone angle values (degree) of TOA^{Me2} and TOA^{tBu} are 230.27° and 236.05°, respectively, and the percentages (%) of the nickel sphere shielded by TOA^{Me2} and TOA^{tBu} are 71.24 and 73.49, respectively. TOA^{Ph} complex 6 formation was confirmed using electrospray ionization-mass (ESI-MS) spectrometry analysis, although its molecular structure has not yet been determined using X-ray crystallographic analysis. Notably, the UV-vis spectral pattern of the TOA^{Ph} complex was more similar to those of the hexa-coordinated TOA^{Me2} complexes $[\text{Ni}(\kappa^2\text{-X})(\text{TOA}^{\text{Me2}})]^+$ (where X = OAc (1) and NO₃ (2)) and $[\text{Ni}(\kappa^1\text{-OC(=O)C}_6\text{H}_4\text{-meta-Cl})(\text{H}_2\text{O})(\text{TOA}^{\text{Me2}})]^+$ (3) than those of the penta-coordinated chlorido complexes with TOA^{Me2} (4) and TOA^{tBu} (5) (Fig. S1†). In fact, elemental analysis data for the TOA^{Ph} complex, which was synthesized by the mixing of TOA^{Ph}, NiCl₂·6H₂O and NaBPh₄ in MeOH and then extracting with CH₂Cl₂ (see experimental), was consistent with the formulation $[\text{NiCl}(\text{TOA}^{\text{Ph}})(\text{MeOH})](\text{BPh}_4)$. A broad band at around 3500 cm^{−1} in an IR spectrum might be assigned to the $\nu\text{O-H}$ of MeOH bound to the nickel center (Fig. S3(f)†). Also, the ESI-MS spectra of an MeCN solution of the TOA^{Ph} complex showed that the ion peaks were attributed to the formulation $[\text{NiCl}(\text{TOA}^{\text{Ph}})(\text{MeCN})]^+$ (Fig. S2(f)†). Three phenyl substituent groups in TOA^{Ph} would make a deep pocket, but the coordination sphere of the nickel center of the TOA^{Ph} complex might be larger than that of TOA^{tBu} because of the planar shape of the phenyl group. Therefore, the obtained 6 has a hexa-coordinated nickel(II) center supported by tetradentate TOA^{Ph}, monodentate Cl[−] and the solvent (MeOH).

Catalytic behaviors of the TOA^R complexes

Cyclohexane oxidation with *m*-CPBA has been achieved using various nickel(II) complexes. Therefore, the catalytic activities of a series of TOA^R complexes and the previously reported catalytically active TPA and Tp* complexes (7 and 8)^{17,21} were



Scheme 2 Synthesis of chlorido complexes with TOA^{tBu} (5) and TOA^{Ph} (6).

examined (Table 3). In addition, chlorido complexes with anionic tridentate ligands $[\text{NiCl}(\text{L})]$ in which $\text{L} = \text{Tp}^*$ (9)³¹ and To^{M} (10),³² where To^{M} is a kind of scorpionate ligand comprising 4,4-dimethyloxazoline, were examined (Fig. 3).

The acetato complex with TOA^{Me_2} 1 showed a higher catalytic rate than the TPA complex 7 (Fig. S5†). The electrochemical oxidation potential of 1 was lower than that of 7 as analyzed by the differential pulse voltammetry (DPV) method (Fig. S6†). Therefore, the electron donating ability of oxazoline seems to be higher than that of pyridine, and such a difference in the electronic properties of the tripodal capping ligands (*i.e.* TOA^{Me_2} and TPA) might reflect on the catalytic performance. In the previously reported cyclohexane oxidation with the Ni/*m*-CPBA system, the catalytic reaction rate of the Tp^* complex 8 is higher than that of an analogous complex with an electron-withdrawing bromine containing ligand $\text{Tp}^{*,\text{Br}}$ ($\text{Tp}^{*,\text{Br}} = \text{hydrotris}(3,5\text{-dimethyl-4-bromo-pyrazol-1-yl})\text{borate}$).²¹

The activity of the chlorido- TOA^{Me_2} complex 4 was close to that of the acetato derivative 1, whereas those of the nitrate (2) and *meta*-chlorobenzoate (3) complexes were lower because induction periods were involved at the initial stage of the reaction (Fig. S7†). Similar anionic ligand-dependent activities

were found for a series of nickel(II)-TPA complexes.¹⁸ In addition, the different activities for hydroxo and chloride complexes with Tp^* (8 and 9) highlighted the dependency of the anionic ligands on the catalytic performance (Fig. S8†).

The order of the initial turnover frequencies (TOF) of the chlorido complexes with TOA^{R} was TOA^{Me_2} (4) > TOA^{Ph} (6) \gg TOA^{tBu} (5) as shown in Fig. S9.† This order seems to reflect that the bulkiness of TOA^{R} depends on R, as discussed above. The initial TOF of the TOA^{Ph} complex 6 was almost half that of the TOA^{Me_2} complex 4, although the yields of cyclohexanol (A) and alcohol selectivity ($A/(K + L)$ values) obtained using both catalysts were comparable. Notably, the oxidant utilization efficiencies were very high with these catalysts; the total turnover number (TON) was *ca.* 970 for both catalysts and the theoretical maximum TON was 1000. The low reaction rate and TON of the TOA^{tBu} complex 5 might imply that the steric hindrance of the *tert*-butyl groups of TOA^{tBu} was critical for the oxidant and substrate to access the nickel center.

The activities of the chlorido complexes with anionic tridentate ligands Tp^* (9) and To^{M} (10) were lower than those of the TOA^{R} complexes 4–6. Particularly, the different catalytic activities of TOA^{Me_2} and To^{M} complexes (with the ligands com-

Table 3 Cyclohexane oxidation

Complex	Ligands	Time/min	Products/μmol					TON ^a	A/(K + L)
			A	K	L	Cy-Cl	Ph-Cl		
1	$\text{TOA}^{\text{Me}_2}/\text{OAc}$	10	1481.2	213.0	13.0	114.7	1053.4	967	6.6
2	$\text{TOA}^{\text{Me}_2}/\text{NO}_3$	120	1160.7	185.0	31.9	84.65	660.7	840	5.4
3	$\text{TOA}^{\text{Me}_2}/\text{H}_2\text{O}/\text{OC}(=\text{O})\text{C}_6\text{H}_4\text{-}m\text{-Cl}$	30	1231.1	128.6	30.2	53.1	492.6	801	7.8
4	$\text{TOA}^{\text{Me}_2}/\text{Cl}$	10	1515.4	164.1	11.9	81.3	786.0	974	8.6
5	$\text{TOA}^{\text{tBu}}/\text{Cl}$	180	552.8	49.7	27.0	31.9	286.6	369	7.2
6	$\text{TOA}^{\text{Ph}}/\text{Cl}$	20	1498.5	161.3	15.9	89.28	862.8	971	8.5
7	TPA/OAc	60	1197.8	110.5	59.5	119.3	771.1	829	7.0
8	Tp^*/OH	180	606.3	111.7	41.8	76.0	480.7	495	3.9
9	Tp^*/Cl	180	378.0	34.2	14.4	48.7	234.7	262	7.8
10	$\text{To}^{\text{M}}/\text{Cl}$	180	370.2	39.3	14.5	31.1	202.4	254	6.9

^a TON = $(A + 2 \times K + 2 \times L + \text{Cy-Cl})/\text{nickel}$.

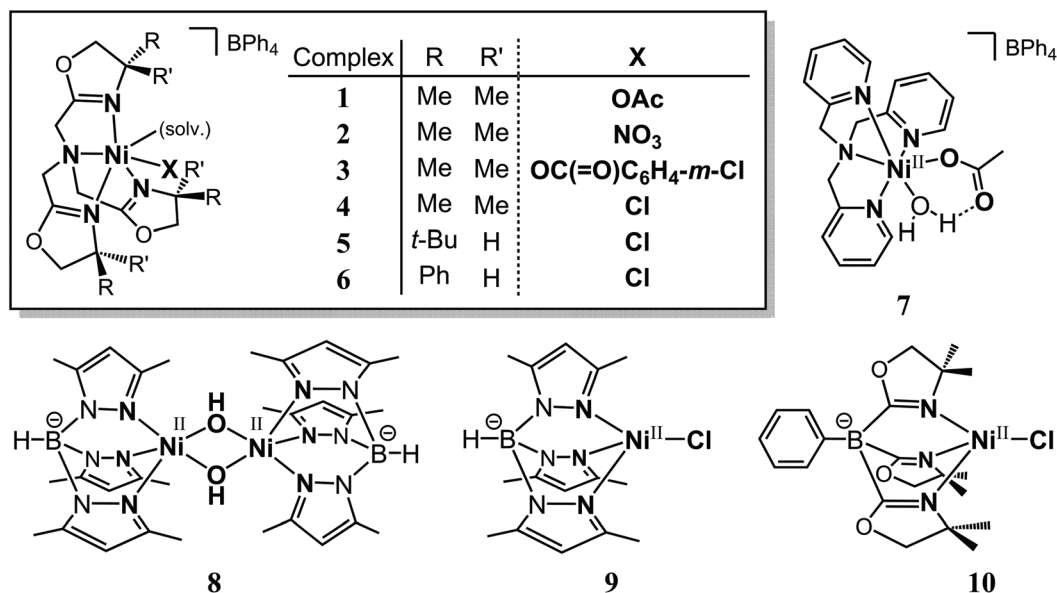


Fig. 3 Complexes applied to the catalytic cyclohexane oxidation with *m*-CPBA.

prising 4,4-dimethyl oxazoline) suggest that an additional amine nitrogen donor on TOA^{Me2} (resulting in the tetradentate chelating ligand) enhances electron donation to induce the activation of the O–O bond of *m*-CPBA. Regarding the anionic tridentate ligands, however, the electron donating ability of To^M is higher than that of Tp^{*}³³ and the catalytic activity of [Co^{II}(acac)(To^M)] toward cyclohexane hydroxylation with *m*-CPBA is higher than that of [Co^{II}(acac)(Tp^{*})].¹⁶ The catalytic activities of the nickel(II)–chlorido complexes **9** and **10** were, however, comparable. Previous reports on the comparison between the metal complexes with To^M and Tp^{*} demonstrate that the calculated equivalent cone angles of To^M are larger

than those of Tp^{*}.³² Therefore, the electronic properties suggest that the intrinsic activity of the nickel(II)–chlorido complex with To^M (**10**) will be higher than that of the Tp^{*} derivative **9**, but the steric hindrance arising from the six methyl groups surrounding the nickel center in **10** prevents the oxidant and substrate from accessing the nickel center.

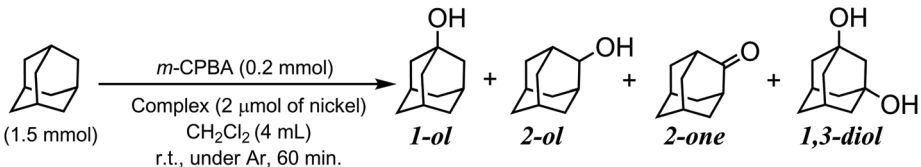
The substituent effect on TOA^R toward the selectivity of the substrate oxidizing position was investigated using the bulky substrates methylcyclohexane (Table 4) and adamantane (Table 5), which involve primary, secondary and tertiary C–H groups. Regarding the oxidation of methylcyclohexane with *m*-CPBA by the chlorido complexes **4**–**6** shown in Table 4, the

Table 4 Methylcyclohexane oxidation

Products/μmol									
Complex	3°-ol	o-2°-ol	m-2°-ol	p-2°-ol	2°-ones	1°-ol	TON ^a	3°-ol : 2°-ols	3°/2° ^b
4	47.7	20.2	21.8	8.6	4.3	0.5	54	49 : 51	8.7
5	33.6	15.4	17.1	8.1	2.9	0.4	40	45 : 55	7.7
6	45.1	19.7	19.9	10.2	5.3	0.4	53	48 : 52	8.2
None ^{c,d}	6.1	0.9	0	0	Trace	0	—	77 : 23	67.8
None ^{c,e}	153.6	10.4	11.5	6.6	2.4	0.2	—	84 : 16	49.7

^a TON = (3°-ol + 2°-ols + 2 × 2°-ones + 1°-ol)/nickel. ^b 3°/2° = (10 × 3°-ol)/(o-2°-ol + m-2°-ol + p-2°-ol + 2°-ones). ^c From ref. 21. ^d Reaction conditions: 13.0 mmol of methylcyclohexane, 0.26 mmol of *m*-CPBA, 1 mL of CH₂Cl₂, 40 °C, 60 min. ^e Reaction conditions: 13.0 mmol of methylcyclohexane, 0.26 mmol of *m*-CPBA, without solvent, 80 °C, 120 min.

Table 5 Adamantane oxidation

						
Complex.	Products/μmol				TON ^a	3°/2° ^b
	1-ol	2-ol	2-one	1,3-diol		
4	95.44	14.58	0.90	0.57	57	18.7
5	73.62	16.53	0.86	0.46	46	12.9
6	79.64	13.81	1.14	0.54	48	16.2
None	11.48	2.07	2.07	0.19	—	8.6

^a TON = (1-ol + 2 × 1,3-diol + 2-ol + 2 × 2-one)/nickel. ^b 3°/2° = [3 × (1-ol + 1,3-diol × 2)]/(2-ol + 2-one).

total amount of secondary C–H oxidized products was greater than the tertiary C–H oxidized alcohol, although the tertiary C–H oxidation occurred mainly without the catalyst.²¹ The tertiary C–H bond of methylcyclohexane is sterically crowded. Therefore, the bulky ligand catalyst favors the oxidation of the less hindered secondary C–H, although the bond dissociation energy (BDE) of the secondary C–H is higher than that of the tertiary C–H. The order of total TON and 3°/2° values (selectivity of the tertiary alcohols normalized by the number of hydrogen atoms attached on the carbon) was R = Me₂ (4) > Ph (6) > *t*Bu (5) of TOA^R.

As shown in Table 5, the same trend of the order of TON and d3°/2° values of the TOA^R complexes (4 > 6 > 5) was observed for adamantane oxidation. The 3°/2° value of *m*-CPBA itself (without the catalyst) toward adamantane was close to that of the *tert*-butoxyl radical (generated *via* the homolysis of O–O of *tert*-BuOOH)³⁴ while smaller than the 3°/2° values in the presence of the catalysts. Upon methylcyclohexane oxidation, however, the 3°/2° values of *m*-CPBA (without catalyst) were larger than those of the TOA^R complexes. Regarding adamantane oxidation, the small 3°/2° value implies the strong oxidative power of the oxidant as supported by the small value (around 2) of the indiscriminate hydroxyl radical. Also, the 3°/2° value is correlated with the radical character of the oxidant as suggested by the large 3°/2° values of iron-oxo species with porphyrin ligands.³⁴ The difference in the magnitude relationship of the 3°/2° values between the *m*-CPBA (without the catalyst) and the TOA^R complexes depending on the substrates might indicate that the 3°/2° value depends not only on the nature of the oxidant but also on the steric hindrance of the substrates.

To obtain insights into the nature of the active species, C₆D₁₂ and toluene oxidation by the acetato complexes with TOA^{Me2} (1) and TPA (7) was examined (Tables S1 and S2†). Regarding C₆D₁₂ oxidation, the kinetic isotope effect (KIE) estimated using cyclohexanol yields on the TOA^{Me2} complex 1 (2.67) was lower than that estimated using the TPA complex 7 (3.74). Toluene oxidation yielded not only oxygenated com-

pounds (benzyl alcohol and benzaldehyde) but also many coupling products arising from the benzyl radical. Notably, the 1,2-diphenylethane (bibenzyl; the homo-coupling product of the benzyl radical) yield obtained using the TOA^{Me2} complex 1 was higher than that obtained using the TPA complex 7. These observations suggest that the radical character of the active species formed on the TOA^{Me2} catalyst is stronger than that formed on the TPA catalyst.

Detection of the acylperoxide adduct on nickel and the kinetic study

We previously characterized the acylperoxido complexes of nickel(II) supported by Tp^R.^{21,22} In this study, reactions of 1 with *m*-CPBA in the absence of the substrate were monitored using spectroscopy.

The cold-spray ionization-mass (CSI-MS) spectra of the mixture of the acetato complex 1 and *m*-CPBA showed ion peaks attributed to an acylperoxido adduct [Ni(OOC(=O)C₆H₄-*meta*-Cl)(TOA^{Me2})]⁺. In addition, the ion peaks of the *meta*-chlorobenzoato (3 - H₂O - BPh₄) and the chlorido (4 - BPh₄) complexes, which are putative decomposed products resulting from the nickel-acylperoxido species, were observed even in the analysis of the solution immediately after mixing 1 and *m*-CPBA (Fig. 4(a)). In the Tp^R complexes, the formation of the chlorido complex was observed during the decomposition of the acylperoxido complex in the presence of CH₂Cl₂.²¹ The ion peaks of the acylperoxido adduct and 1 disappeared later (Fig. 4(b)).

Acylperoxido adduct formation was also observed using UV-vis spectroscopy. Adding one equivalent of *m*-CPBA to the CH₂Cl₂ solution of 1 at 10 °C caused an increase in the absorption band at 398 nm (Fig. 5). This band decayed gradually at the same temperature and was accelerated by adding xanthene. Therefore, the absorption band at 398 nm was assigned to the acylperoxido complex. Pseudo-first order reaction rates (= *k*_{obs}) for acylperoxido complex decay were saturated by increasing the concentration of xanthene, which implies that the reaction proceeds through a Michaelis-

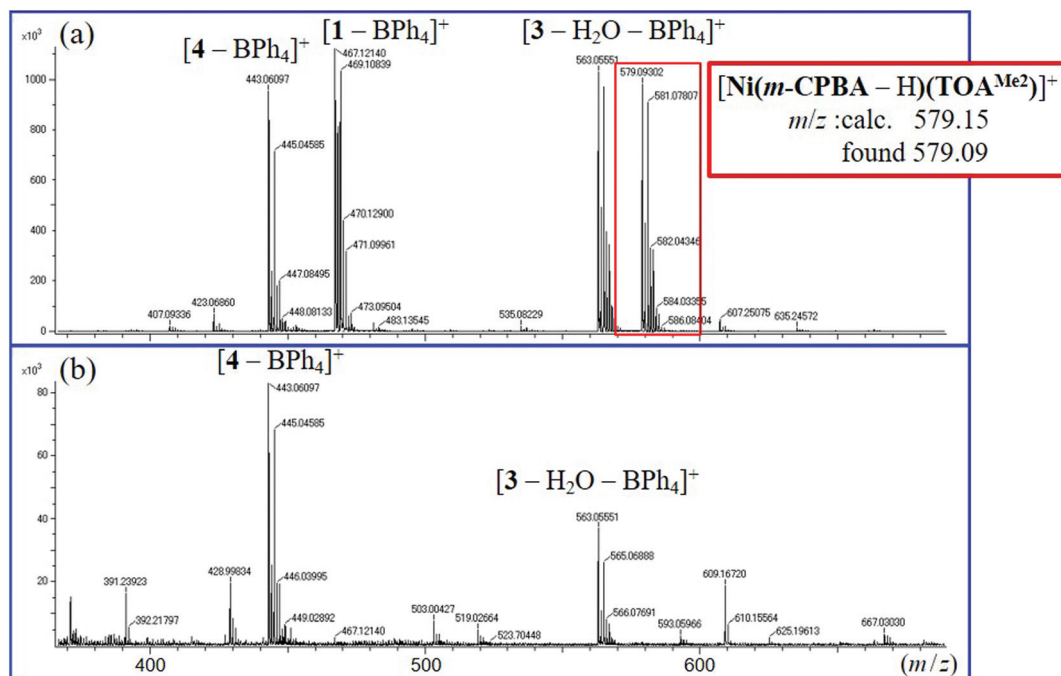


Fig. 4 Cold-spray ionization mass (CSI-MS) spectra of the reaction mixture of **1** and *m*-CPBA in CH₂Cl₂ at room temperature. (a) Measured immediately after mixing **1** and *m*-CPBA. (b) Measured after one day at ambient temperature.

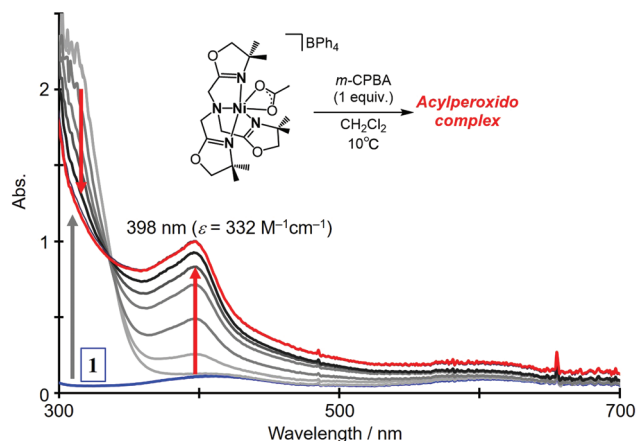


Fig. 5 UV-vis spectra of the reaction of **1** and *m*-CPBA in CH₂Cl₂ at 10 °C.

Menten type mechanism (Fig. 6). In the presence of cyclohexane, however, *m*-CPBA complex decay was not accelerated. Notably, the decay of the acylperoxido species of the Tp*-nickel system exhibited the KIE depending on the solvents CH₂Cl₂ and CD₂Cl₂.²¹ In the present TOA^{Me2} complex, no KIE was observed, as evidenced by the fact that the first-order decay rates at 25 °C were 1.31 × 10⁻⁴ s⁻¹ in CH₂Cl₂ and 1.03 × 10⁻⁴ s⁻¹ in CD₂Cl₂ (Fig. S10†). These observations suggest that the acylperoxido complex with TOA^{Me2} is a precursor of the active species for the oxidation of high C-H BDE substrates, although the low C-H BDE substrates can be oxidized directly by the

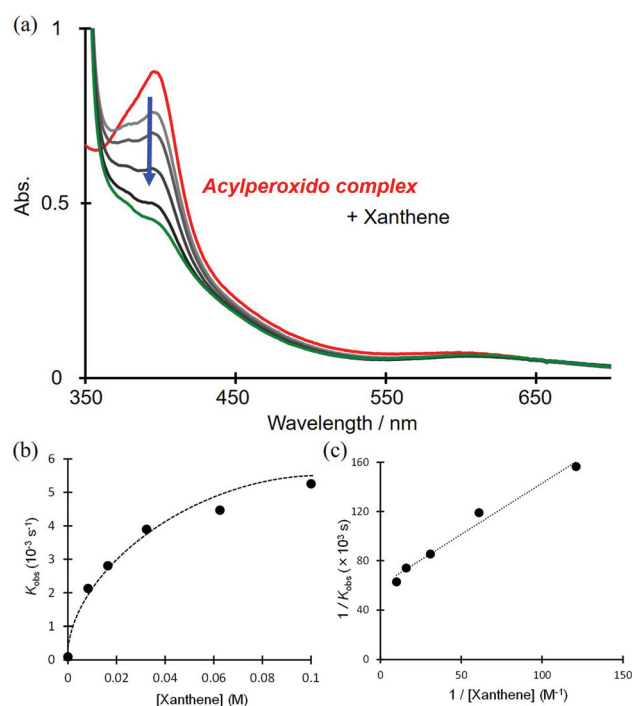


Fig. 6 Reaction of the acylperoxido complex and xanthene in CH₂Cl₂ at 10 °C. (a) Reaction monitored by UV-vis spectroscopy. (b) Plot of the pseudo-first order decay rates of the acylperoxido complex versus the concentration of xanthene. (c) Lineweaver-Burk plot.

acylperoxido complex. Some nickel-oxo or/and oxyl species formed through O–O bond activation of *m*-CPBA have been reported.^{35–37} In the presented system, the O–O bond of the coordinated acylperoxide might be activated to obtain nickel(II) or nickel(III)-oxyl species as real active species for alkane oxidation.

Conclusion

Nickel(II) complexes with oxazoline donors containing tertiary amine ligands, TOA^R, were synthesized. X-ray crystallographic analysis of the TOA^{Me2} complexes revealed that the TOA^{Me2} ligand acted as the tripodal tetradentate chelating reagent to support the mononuclear nickel(II) center. The shape and bulkiness of the substituent groups R on the fourth position of the oxazoline rings affect the coordination environment of the nickel centers.

The TOA^R complexes of nickel(II) efficiently catalyze the oxidation of alkane with *m*-CPBA. The catalytic activity of the acetate–nickel complex with TOA^{Me2} was higher than that of the TPA analogue because of the oxazoline's strong σ -donating nature. The steric hindrance derived from the R on TOA^R affects the catalytic reaction rate and the selectivity of the products. The catalytic reaction might proceed through the nickel(II)-acylperoxido species, which could be detected using spectroscopy. In the present TOA^R–Ni system, the acylperoxido complex might be a precursor of the active species for alkane oxidation.

Experimental section

General

All manipulations were performed under argon using standard Schlenk techniques. THF, toluene, CH₂Cl₂ and MeCN were purified over a Glass Contour Solvent Dispensing System under an Ar atmosphere. *meta*-Chloroperoxybenzoic acid (*m*-CPBA) was washed with KH₂PO₄–NaOH buffer solution (pH 7.4) and pure water to remove *meta*-chlorobenzoic acid. Other reagents of the highest commercially available grade were used without further purification. The ligands TOA^{Me2},²⁹ TOA^{tBu} and TOA^{Ph},¹¹ and the catalyst precursors [Ni(OAc)(H₂O)(TPA)](BPh₄) (7),^{17,18} [(Ni^{II}TP*)₂(μ -OH)₂] (8),³⁸ [NiCl(Tp*)] (9)³¹ and [NiCl(To^M)] (10)³² were prepared using methods described in the literature.

Elemental analyses were performed using an Elementar Vario Micro Cube. The IR measurements of KBr pellets of solid compounds were conducted using JASCO FT/IR 4200 spectrometers. UV/vis spectra were recorded on a JASCO V650 or Agilent 8453 spectrometer equipped with a UNISOKU CoolSpeK USP-203-A for low-temperature measurements. Mass spectra were recorded on a JEOL JMS-T100LC using electrospray ionization (ESI) and cold-spray ionization (CSI). ¹H NMR spectra were recorded on a JEOL EX-500. Differential pulse voltammograms were measured on a Hokuto Denko

Electrochemical Measurement System HZ-7000. Gas chromatography (GC) analyses were conducted on Shimadzu GC-2010 and GC-2025 instruments with a flame ionization detector equipped with Restek Rtx-5 (on GC-2010) and Rtx-WAX (on GC-2025) capillary columns (Restek, length = 30 m, i.d. = 0.25 mm, thickness = 0.25 μ m). GC-MS analyses were conducted on a Shimadzu PARVUM2 system equipped with a RESTEK Rtx-5MS capillary column (Restek, length = 30 m, i.d. = 0.25 mm, thickness = 0.25 μ m).

Synthesis of TOA^{Me2} complexes

The acetato (1), nitrate (2) and chloride (4) complexes with TOA^{Me2} were synthesized using the same procedures. The *meta*-chlorobenzoato complex 3 was synthesized from 2 using a ligand exchange reaction.

[Ni^{II}(OAc)(TOA^{Me2})](BPh₄) (1). As a typical example, the synthetic procedure for the acetato complex 1 is described. A methanol solution (10 mL) of TOA^{Me2} (1.51 g; 4.30 mmol) was added to a methanol solution (15 mL) of Ni(OAc)₂·4H₂O (1.00 g; 4.02 mmol) at RT and the solution was stirred for 30 min. Addition of NaBPh₄ (1.65 g; 4.83 mmol) to this blue-green solution led to the precipitation of a blue-green powder. The resulting powder was collected by filtration and recrystallized by the slow diffusion of CH₂Cl₂/*n*-hexane yielding blue-green crystals of 1 (1.43 g, 45% yield). FT-IR (KBr): ν = 3056, 3033, 2981, 2940, 1945, 1886, 1824, 1675, 1579, 1540, 1461, 1419, 1369, 1306, 1307, 1274, 1064, 1008, 950, 889, 842, 734, 707, 686, 611 cm^{−1}. ESI-MS (positive, MeCN): m/z = 467.1 [Ni + TOA^{Me2} + OAc]⁺. UV-vis (CH₂Cl₂): λ (ϵ) = 411 (21), 609 (14), 799 nm (3.2). Elemental analysis: calcd (%) for [C₂₀H₃₃N₄NiO₅] (C₂₄H₂₀B) C: 67.11, H: 6.78, N: 7.12; found C: 67.16, H: 6.79, N: 7.24.

[Ni^{II}(NO₃)(TOA^{Me2})](BPh₄) (2). Green crystals of 2 (1.20 g; 1.36 mmol; 47% yield) were obtained by re-crystallization of the corresponding crude yellow-green powder that was synthesized by reacting Ni(NO₃)₂·6H₂O (0.84 g; 2.89 mmol) and TOA^{Me2} (1.03 g; 2.92 mmol) in methanol and adding NaBPh₄ (1.15 g; 3.36 mmol). FT-IR (KBr): ν = 3056, 2983, 1669, 1653, 1579, 1477, 1420, 1384, 1276, 1204, 1120, 1064, 1012, 955, 884, 841, 810, 734, 707, 645, 612 cm^{−1}. ESI-MS (positive, MeCN): m/z = 470.2 [Ni + TOA^{Me2} + NO₃]⁺. UV-vis (CH₂Cl₂): λ (ϵ) = 402 (25), 610 (20), 800 nm (4.5). Elemental analysis: calcd (%) for [C₁₈H₃₀N₅NiO₆](C₂₄H₂₀B)·1.5CH₂Cl₂ C: 56.93, H: 5.82, N: 7.63; found C: 57.13, H: 5.48, N: 7.70.

[Ni^{II}(Cl)(TOA^{Me2})](BPh₄) (4). Orange crystals of 4 (0.641 g; 0.839 mmol; 63% yield) were obtained by re-crystallizing the corresponding crude orange powder that was synthesized by reacting NiCl₂·6H₂O (0.320 g; 1.35 mmol) and TOA^{Me2} (0.468 g; 1.33 mmol) in methanol and adding NaBPh₄ (0.468 g; 1.35 mmol). FT-IR (KBr): ν = 3055, 2998, 2983, 2937, 1953, 1889, 1821, 1667, 1650, 1578, 1560, 1468, 1422, 1386, 1369, 1312, 1276, 1206, 1183, 1125, 1064, 1014, 957, 886, 843, 733, 706, 643, 611 cm^{−1}. ESI-MS (positive, MeCN): m/z = 443.1 [Ni + TOA^{Me2} + Cl]⁺. UV-vis (CH₂Cl₂): λ (ϵ) = 465 (79), 732 nm (23). Elemental analysis: calcd (%) for [C₁₈H₃₀N₄ClNiO₃](C₂₄H₂₀B) C: 66.04, H: 6.60, N: 7.34; found C: 65.69, H: 6.74, N: 7.59.

[Ni^{II}(O₂CC₆H₄-*meta*-Cl)(H₂O)(TOA^{Me2})](BPh₄) (**3**). The potassium salt of *meta*-chlorobenzoic acid (2.38 mg; 0.121 mmol) was added to a CH₂Cl₂ solution (10 mL) of the nitrato complex **2** (92.4 mg; 0.117 mmol) at RT and the resulting suspension was stirred for 12 h. After the removal of insoluble compounds by filtration through a Celite pad, volatiles were evaporated from the filtrate to give a pale blue solid. Recrystallizing the crude product from the CH₂Cl₂/*n*-hexane mixture yielded pale blue needle-shaped crystals of **3** (69.5 mg, 0.0750 mmol; 64%). FT-IR (KBr): ν = 3605, 2970, 1677, 1558, 1457, 1419, 1375, 1274, 1201, 1010, 953, 731, 708, 611 cm⁻¹. ESI-MS (positive, MeCN): m/z = 563.2 [Ni + TOA^{Me2} + O₂CC₆H₄-*meta*-Cl]⁺. UV-vis (CH₂Cl₂): λ (ε) = 412 (26), 612 (17), 800 nm (5.2). Elemental analysis: calcd (%) for [C₂₅H₃₄N₄ClNiO₅](C₂₄H₂₀B)-0.5CH₂Cl₂ C: 64.18, H: 5.98, N: 6.05; found C: 64.22, H: 6.12, N: 6.04.

Synthesis of [Ni^{II}(Cl)(TOA^{tBu})](BPh₄) (5**).** A methanol solution (10 mL) of TOA^{tBu} (0.287 g; 1.21 mmol) was added to a methanol solution (15 mL) of NiCl₂·6H₂O (0.506 g; 1.16 mmol) at RT and the solution was stirred for 30 min. Adding NaBPh₄ (0.417 g; 1.22 mmol) to this solution precipitated a pink powder. The powder was collected by filtration and recrystallized by the slow diffusion of CH₂Cl₂/*n*-hexane yielding red block-shaped crystals of **5** (0.217 g, 0.257 mmol; 22% yield). FT-IR (KBr): ν = 3056, 3031, 2962, 2871, 1941, 1880, 1818, 1654, 1633, 1579, 1477, 1423, 1369, 1349, 1301, 1228, 1124, 997, 956, 925, 877, 848, 809, 736, 703, 611 cm⁻¹. ESI-MS (positive, MeCN): m/z = 518.3 [Ni + TOA^{tBu} + CN]⁺. UV-vis (CH₂Cl₂): λ (ε) = 470 (64), 723 (17), 829 nm (11). Elemental analysis: calcd (%) for [C₂₄H₃₉N₄ClNiO₃](C₂₄H₂₀B) C: 68.23, H: 7.04, N: 6.63; found C: 67.70, H: 7.39, N: 6.56.

Synthesis of [Ni^{II}(Cl)(TOA^{Ph})(MeOH)](BPh₄) (6**).** A methanol solution (5 mL) of TOA^{Ph} (0.567 g; 1.15 mmol) was added to a methanol solution (5 mL) of NiCl₂·6H₂O (0.274 g; 1.15 mmol) at RT and the solution was stirred for 15 min. NaBPh₄ (0.401 g; 1.17 mmol) was then added to this solution and stirred for 30 min. No compounds were precipitated. After the removal of volatiles by evaporation, the resulting crude green powder was suspended in CH₂Cl₂ and the insoluble compounds were removed by filtration through a Celite pad. CH₂Cl₂ evaporation from the filtrate yielded a yellow green powder of **6** (0.424 g; 0.47 mmol; 41% yield). The resulting compound was applied to catalytic tests without further purification. FT-IR (KBr): ν = 3326, 3054, 1955, 1884, 1818, 1679, 1633, 1577, 1544, 1473, 1452, 1411, 1307, 1268, 1232, 1122, 1029, 969, 931, 881, 842, 734, 703, 638, 611 cm⁻¹. ESI-MS (positive, MeCN): m/z = 587.1 [Ni + TOA^{Ph} + Cl]⁺. UV-vis (CH₂Cl₂): λ (ε) = 401 (46), 663 nm (20). Elemental analysis: calcd (%) for [C₃₁H₃₁N₄ClNiO₄](C₂₄H₂₀B) C: 70.50, H: 5.49, N: 5.98; found C: 70.45, H: 5.85, N: 5.40.

Crystallographic analysis

Diffraction data for single crystals were collected using a Rigaku Saturn 70 CDD area detector system with graphite monochromated Mo-K α radiation. Data collection was conducted at 293 K for **1**, 113 K for **2–4** and 133 K for **5**.

Data collection and processing were performed using Rigaku CrystalClear software.³⁹ Structural solution by direct methods (SIR-92)⁴⁰ and refinement by full-matrix least squares (SHELXL-2014/7)⁴¹ against F^2 with all reflections were performed using WinGX⁴² software. All non-hydrogen atoms were refined anisotropically. Hydrogen atoms adjacent to carbon atoms were placed in calculated positions with C–H = 0.98 Å for methyl groups, 0.99 Å for methylene groups and 0.95 Å for aromatic rings with $U_{iso}(H) = 1.2U_{iso}$ (attached atom). The molecular structures were drawn using ORTEP-3 for Windows.⁴³ The Crystallographic Information Files (CIF) of the complexes reported in this paper have been deposited with the Cambridge Crystallographic Data Centre as supplementary publications CCDC 1983778–1983782.†

Catalytic oxidation of substrates with *m*-CPBA

All reactions were conducted at room temperature under Ar and the products were analyzed quantitatively using GC with an internal standard.

Cyclohexane oxidation. A solution of the nickel(II) compounds (2.0 μmol of **1–7**, **9** and **10** and 1.0 μmol of **8**, that is, 2.0 μmol of nickel(II)), cyclohexane (15.0 mmol) and nitrobenzene (0.10 mmol; as an internal standard for quantitative analysis by GC) in a mixture of MeCN (1 mL) and CH₂Cl₂ (1 mL) was placed in a Schlenk flask and degassed with Ar gas. Next, a CH₂Cl₂ (2 mL) solution of *m*-CPBA (2.0 mmol) was added under an Ar atmosphere and stirred at room temperature. To monitor product formation, 0.1 mL of the reaction mixture was corrected at certain times (reaction times 0, 10, 20, 30, 60, 120, 180 min) and quenched with a dichloromethane solution (0.5 mL) of triphenylphosphine (10 mg) and then the solution was subjected to GC analysis (GC-2010 equipped with an Rtx-5 capillary column).

Methylcyclohexane oxidation. The chloride complexes with TOA^R **4–6** were applied as catalyst precursors. The procedure for the oxidation reaction was the same as for cyclohexane oxidation except for the amount of *m*-CPBA (0.20 mmol applied). In addition, a GC-2025 equipped with an Rtx-WAX capillary column was used for product analysis.

Adamantane oxidation. The reaction conditions were essentially the same as for methylcyclohexane oxidation except for the solvent (sole CH₂Cl₂ instead of a mixture of CH₂Cl₂ and MeCN) and amount of substrate (1.5 mmol).

Toluene oxidation. Prior to GC analysis, the oxygenated products (benzyl alcohol and benzaldehyde) were trimethylsilylated with a mixture of silylation reagents prepared by mixing trimethylchlorosilane (0.1 mL) and hexamethyldisilazane (0.3 mL) in anhydrous pyridine (0.9 mL). The acetato complexes were applied as catalyst precursors. A solution of 2.0 μmol of the acetato complexes with TOA^{Me2} (**1**) or TPA (**7**), toluene (15.0 mmol) and nitrobenzene (0.10 mmol; as an internal standard for quantitative analysis by GC) in a mixture of MeCN (1 mL) and CH₂Cl₂ (1 mL) was placed in a Schlenk flask and degassed with Ar gas. Next, a CH₂Cl₂ (2 mL) solution of *m*-CPBA (0.20 mmol) was added under an Ar atmosphere and stirred at room temperature. After 60 min, 0.1 mL

of the reaction mixture was collected and quenched with a dichloromethane solution (0.5 mL) of triphenylphosphine (10 mg) containing 0.1 mL of the silylation reagent mixture. The solution was analyzed using GC-MS for quantitative analysis of the products and GC for quantitative analysis of the trimethylsilylated oxygenated products and 1,2-diphenylethane on a GC-2010 equipped with an Rtx-5 capillary column.

Conflicts of interest

There are no conflicts to declare.

Acknowledgements

This research was funded by CREST, JST (JPMJCR16P1) and Kanagawa University (ordinary budget: 411).

References

- 1 M. Hoogenraad, K. Ramkisoensing, S. Gorter, W. L. Driessen, E. Bouwman, J. G. Haasnoot, J. Reedijk, T. Mahabiersing and F. Hartl, *Eur. J. Inorg. Chem.*, 2002, 377–387.
- 2 M. Hoogenraad, H. Kooijman, A. L. Spek, E. Bouwman, J. G. Haasnoot and J. Reedijk, *Eur. J. Inorg. Chem.*, 2002, 2897–2903.
- 3 M. Bagherzadeh, R. Latifi and L. Tasini, *J. Mol. Catal. A: Chem.*, 2006, **260**, 163–169.
- 4 M. D. Godbole, M. P. Puig, S. Tanase, H. Kooijman, A. L. Spek and E. Bouwman, *Inorg. Chim. Acta*, 2007, **360**, 1954–1960.
- 5 M. Bagherzadeh, M. Amini, A. Ellern and L. K. Woo, *Inorg. Chem. Commun.*, 2012, **15**, 52–55.
- 6 M. Gómez, S. Jansat, G. Muller, G. Noguera, H. Teruel, V. Moliner, E. Cerrada and M. Hursthouse, *Eur. J. Inorg. Chem.*, 2001, 1071–1076.
- 7 J. A. Brito, M. Gómez, G. Muller, H. Teruel, J.-C. Clinet, E. Duñach and M. A. Maestro, *Eur. J. Inorg. Chem.*, 2004, 4278–4285.
- 8 B. W. Michel, L. D. Steffens and M. S. Sigman, *J. Am. Chem. Soc.*, 2011, **133**, 8317–8325.
- 9 J. Arias, C. R. Newlands and M. M. Abu-Omar, *Inorg. Chem.*, 2001, **40**, 2185–2192.
- 10 T. Niwa and M. Nakada, *J. Am. Chem. Soc.*, 2012, **134**, 13538–13541.
- 11 K. Kawasaki and T. Katsuki, *Tetrahedron*, 1997, **53**, 6337–6350.
- 12 Y. Kohmura and T. Katsuki, *Tetrahedron Lett.*, 2000, **41**, 3941–3945.
- 13 M. B. Andrus and Z. Zhou, *J. Am. Chem. Soc.*, 2002, **124**, 8806–8807.
- 14 V. Köhler, C. Mazet, A. Toussaint, K. Kulicke, D. Häussinger, M. Neuburger, S. Schaffner, S. Kaiser and A. Pfaltz, *Chem. – Eur. J.*, 2008, **14**, 8530–8539.
- 15 R. R. Reinig, D. Mukherjee, Z. B. Weinstein, W. Xie, T. Albright, B. Baird, T. S. Gray, A. Ellern, G. J. Miller, A. H. Winter, S. L. Bud'ko and A. D. Sadow, *Eur. J. Inorg. Chem.*, 2016, 2486–2494.
- 16 T. Nishiura, T. Uramoto, Y. Takiyama, J. Nakazawa and S. Hikichi, *Molecules*, 2018, **23**, 1466.
- 17 T. Nagataki, Y. Tachi and S. Itoh, *Chem. Commun.*, 2006, 4016–4018.
- 18 T. Nagataki, K. Ishii, Y. Tachi and S. Itoh, *Dalton Trans.*, 2007, 1120–1128.
- 19 T. Nagataki and S. Itoh, *Chem. Lett.*, 2007, **36**, 748–749.
- 20 M. Balamurugan, R. Mayilmurugan, E. Suresh and M. Palaniandavar, *Dalton Trans.*, 2011, **40**, 9413–9424.
- 21 S. Hikichi, K. Hanaue, T. Fujimura, H. Okuda, J. Nakazawa, Y. Ohzu, C. Kobayashi and M. Akita, *Dalton Trans.*, 2013, **42**, 3346–3356.
- 22 J. Nakazawa, S. Terada, M. Yamada and S. Hikichi, *J. Am. Chem. Soc.*, 2013, **135**, 6010–6013.
- 23 E. Tordin, M. List, U. Monkowius, S. Schindler and G. Knor, *Inorg. Chim. Acta*, 2013, **402**, 90–96.
- 24 M. Sankaralingam, P. Vadivelu, E. Suresh and M. Palaniandavar, *Inorg. Chim. Acta*, 2013, **407**, 98–107.
- 25 (a) J. Nakazawa, T. Hori, T. D. P. Stack and S. Hikichi, *Chem. – Asian J.*, 2013, **8**, 1191–1199; (b) J. Nakazawa, Y. Doi and S. Hikichi, *Mol. Catal.*, 2017, **443**, 14–24.
- 26 M. Sankaralingam, M. Balamurugan, P. Vadivelu, C. H. Suresh and M. Palaniandavar, *Chem. – Eur. J.*, 2014, **20**, 11346–11361.
- 27 M. Sankaralingam, P. Vadivelu and M. Palaniandavar, *Dalton Trans.*, 2017, **46**, 7181–7193.
- 28 (a) T. Bodner, L. Ellmaier, V. Schenk, J. Albering and F. Wiesbrock, *Polym. Int.*, 2011, **60**, 1173–1179; (b) M. Fimberger, K. P. Luef, C. Payerl, R. C. Fischer, F. Stelzer, M. Kállay and F. Wiesbrock, *Materials*, 2015, **8**, 5385–5397.
- 29 T. N. Sorrell, F. C. Pigge and P. S. White, *Inorg. Chim. Acta*, 1993, **210**, 87–90.
- 30 I. A. Guzei and M. Wendt, *Dalton Trans.*, 2006, 3991–3999.
- 31 P. J. Desrochers, S. LeLievre, R. J. Johnson, B. T. Lamb, A. L. Phelps, A. W. Cordes, W. Gu and S. P. Cramer, *Inorg. Chem.*, 2003, **42**, 7945–7950.
- 32 T. Takayama, J. Nakazawa and S. Hikichi, *Acta Crystallogr., Sect. C: Struct. Chem.*, 2016, **72**, 842–845.
- 33 K. Wu, D. Mukherjee, A. Ellern, A. D. Sadow and W. E. Geiger, *New J. Chem.*, 2011, **35**, 2169–2178.
- 34 M. Costas, K. Chen and L. Que Jr., *Coord. Chem. Rev.*, 2000, **200–202**, 517–544.
- 35 F. F. Pfaff, F. Heims, S. Kundu, S. Mebs and K. Ray, *Chem. Commun.*, 2012, **48**, 3730–3732.
- 36 T. Corona, F. F. Pfaff, F. Acuna-Pares, A. Draksharapu, C. J. Whiteoak, V. Martin-Diaconescu, J. Lloret-Fillol, W. R. Browne, K. Ray and A. Company, *Chem. – Eur. J.*, 2015, **21**, 15029–15038.

- 37 A. Parrot, Y. Morimoto, S. Paria, H. Sugimoto, N. Fujieda and S. Itoh, *Dalton Trans.*, 2017, **46**, 8013–8016.
- 38 S. Hikichi, M. Yoshizawa, Y. Sasakura, H. Komatsuzaki, Y. Moro-oka and M. Akita, *Chem. –Eur. J.*, 2001, **7**, 5011–5028.
- 39 Rigaku. *CrystalClear*. Rigaku Corporation, Tokyo, Japan, 2008.
- 40 A. Altomare, G. Cascarano, C. Giacovazzo, A. Guagliardi, M. C. Burla, G. Polidori and M. Camalli, *J. Appl. Crystallogr.*, 1994, **27**, 435.
- 41 G. M. Sheldrick, *Acta Crystallogr., Sect. A: Found. Crystallogr.*, 2008, **64**, 112–122.
- 42 L. J. Farrugia, *J. Appl. Crystallogr.*, 1999, **32**, 837–838.
- 43 L. J. Farrugia, *J. Appl. Crystallogr.*, 2012, **45**, 849–854.